Check for updates

Water adsorption on MoS$_2$ under realistic atmosphere conditions and impacts on tribology†

N. Scott Bobbitt, [ID] John F. Curry, [ID] Tomas F. Babuska and Michael Chandross [ID] *

Molybdenum disulfide (MoS$_2$) is a 2D material widely used as a dry lubricant. However, exposure to water and oxygen is known to reduce its effectiveness, and therefore an understanding of the uptake of water is important information for mitigating these effects. Here we use grand canonical Monte Carlo simulations to rigorously study water adsorption on MoS$_2$ surfaces and edges with different concentrations of defects under realistic atmospheric conditions (*i.e.* various temperatures and humidity levels). We find that the amount of water adsorbed depends strongly on the number of defects. Simulations indicate that defect sites are generally saturated with water even at low ppm levels of humidity. Water binds strongly to S vacancies on interlamellar surfaces, but generally only one water molecule can fit on each of these sites. Defects on surfaces or edges of lamellae also strongly attract water molecules that then nucleate small clusters of water bonded *via* hydrogen bonding. We demonstrate that water preferentially binds to surface defects, but once those are saturated at a critical humidity level of about 500–1000 ppm water, water binds to edge sites where it negatively impacts the tribological performance of MoS$_2$.

1 Introduction

Molybdenum disulfide (MoS$_2$) is a lamellar solid consisting of Mo and S in a 2D hexagonal structure.[1–3] MoS$_2$ has been the subject of widespread research for many applications including catalysis,[4–8] chemical sensors,[9–13] and electronic devices.[14–16] Prior to research interest in these areas, MoS$_2$ has been used as a solid lubricant[17–22] in aerospace applications for decades owing to its extremely low friction and resistance to wear at cryogenic temperatures[23] and under vacuum.

The low shear strength and friction of MoS$_2$ are due to its lamellar structure in which thin, stacked layers of MoS$_2$ are held together by relatively weak van der Waals forces that permit layers to easily slide across each other. Previous research has demonstrated that water and other environmental contaminants, such as atmospheric water, oxygen, and adventitious carbon increase friction in MoS$_2$ and reduce desirable lubrication properties.[24–31] This has limited the utility of MoS$_2$ as a lubricant, especially for applications where it is exposed to humidity. Even for devices destined for the vacuum of space, components are constructed and launched from Earth and often exposed to humid air during fabrication and testing, and this can have a negative impact on the effectiveness of MoS$_2$ lubricants.

Considerable research has focused on understanding the precise mechanism through which water impacts the structure and performance of MoS$_2$.[32,33] Previous work from our group has suggested that water adsorbs on the edges of MoS$_2$ flakes, disrupting the lamellar structure and resulting in higher friction.[34–37] Others have suggested increases in friction are due to MoS$_2$ oxidizing to MoO$_3$,[27,28] hydrogen bonding from water,[38,39] or capillary effects.[40]

Despite these efforts to understand the fundamental interactions of MoS$_2$, water, and oxygen, there have not to date been any rigorous efforts to quantify the amount of water adsorbed by MoS$_2$ under realistic atmospheric conditions. In the work presented here, we use atomistic simulations to predict the amount of water adsorbed from a realistic atmosphere at ambient temperatures, similar to those to which MoS$_2$ might be exposed during device fabrication and testing. As S vacancies are the most common defect in MoS$_2$, we specifically consider the impact of varying densities of S vacancies.[41] This work provides a basis for understanding how much water is likely to be adsorbed by MoS$_2$ under realistic conditions.

2 Methods

Grand canonical Monte Carlo (GCMC) simulations were used to compute adsorption isotherms for water, O$_2$, N$_2$, and Ar in MoS$_2$ using the multipurpose molecular simulation code RASPA.[42] The simulation box consisted of eight layers of MoS$_2$ (10 × 10 Mo atoms) that were held fixed. These calculations used Lennard-Jones parameters for MoS$_2$ from Gu *et al.*[43] that were

Material, Physical, and Chemical Sciences Center, Sandia National Laboratories, Albuquerque, New Mexico 87123, USA. E-mail: mechand@sandia.gov

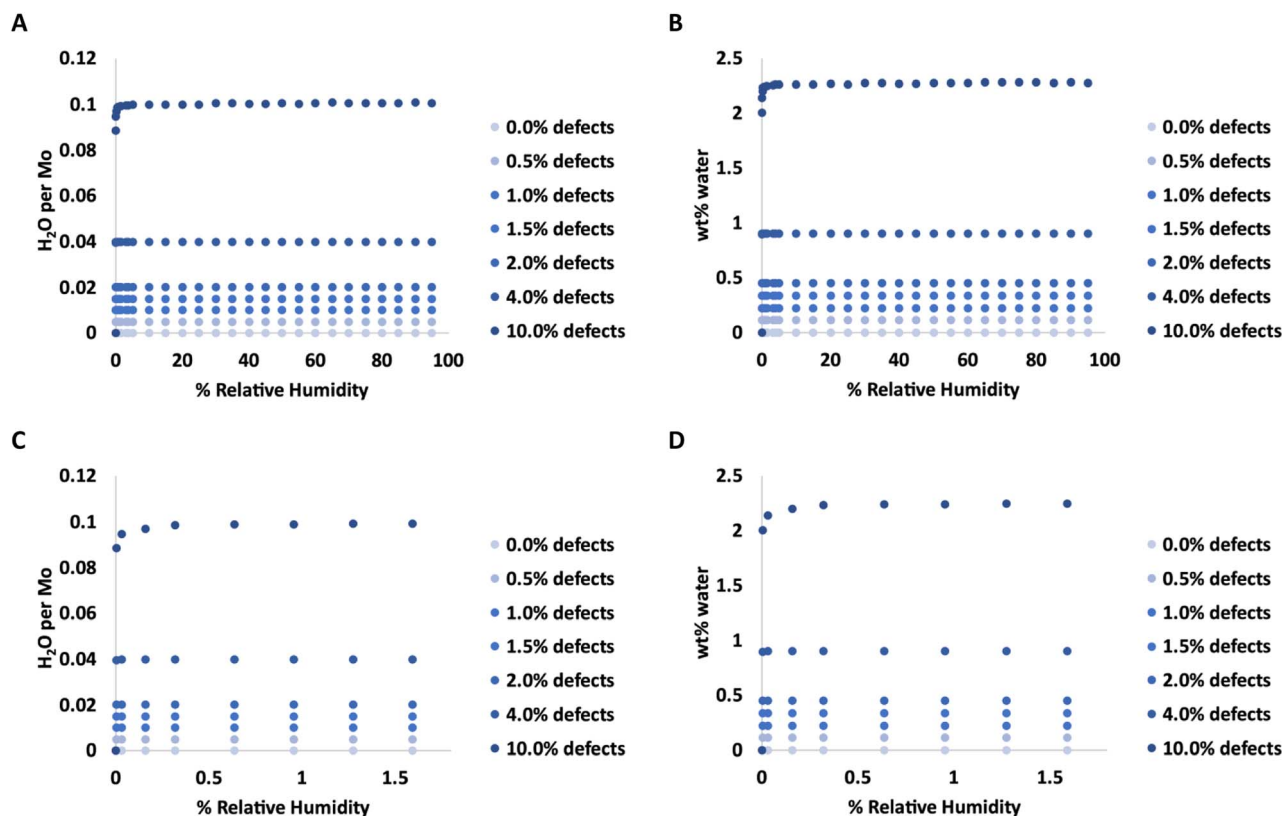† Electronic supplementary information (ESI) available. See DOI: https://doi.org/10.1039/d3ra07984h

Fig. 1 Adsorption isotherms for water in MoS_2 at 298 K with various levels of defects. C and D show the same data as in A and B, respectively, but expanded for low levels of humidity.

developed to accurately capture interactions between MoS_2 and water. The TIP3P model was used for all water interactions,[44] consistent with the Gu model. Partial charges for the MoS_2 were computed using EQeq as implemented in RASPA.[45] Note that while the Gu force field prescribes fixed charges of +0.76 and −0.38 on Mo and S, respectively, calculating dynamic charges allows us to account for changes in the partial charges due to defects. The computed values for charges in pristine MoS_2 using EQeq are about +0.70 on Mo and −0.35 on S, similar to the Gu values.

The TRaPPE model[46] was used for N_2 and O_2, and parameters for Ar were taken from Garcia-Perez.[47] Lennard-Jones interactions were truncated at a cutoff of 12.8 Å with no tail corrections. Cross-terms were treated with mixing rules (arithmetic mean of ε, geometric mean of σ),[48] and Coulomb interactions were treated using the Ewald summation method. The simulation box was at least twice the LJ cutoff (25.6 Å) in all dimensions. GCMC simulations for bulk MoS_2 used 100 000 initialization cycles followed by 200 000 production cycles. GCMC simulations for surfaces or edges used 500 000 initialization cycles and 1 000 000 production cycles. The allowed Monte Carlo moves were translation, rotation, regrowth, insertion, deletion, and identity change, all with equal probability. Simulations were performed at 1 bar (0.1 MPa) and either 278 K, 298 K, or 313 K. The composition of the gas reservoir was chosen to mimic a humid atmosphere, including O_2, N_2, Ar, and

water. For the exact composition used in each simulation, see ESI Table 1.† All Lennard-Jones parameters are given in ESI Table 3.† MoS_2 unit cell parameters (for 2H phase) are given in ESI.†

Defects were created by randomly removing S atoms to create a specific defect density, followed by a recalculation of the partial charges in RASPA. The MoS_2 structure was held fixed at the crystallographic minimum computed with density functional theory (DFT) (PAW_PBE pseudopotentials, 520 eV energy cutoff, and a 4 × 4 × 1 Monkhorst–Pack k-points grid) in our previous work.[37] The energy of separating layers of MoS_2 was computed using single point DFT calculations with the same parameters.

Friction experiments were carried out on a custom linear reciprocating microtribometer in both rough vacuum environments (∼2 torr) and ambient pressure to achieve a wide range of partial pressures of water, ranging from 0.054 to 5.624 torr. Partial pressures of water and other environmental constituents were measured via an ambient pressure residual gas analyzer with an orifice plate for operation in 2 torr, alongside a chilled mirror hygrometer to measure partial pressures of water in ambient conditions. All friction experiments were carried out for 500 sliding cycles on 1 micron thick physical vapor deposited MoS_2 coatings against a 1/8″ diameter steel counterface at 200 mN load, 1 mm s^{-1} sliding speed and 2 mm stroke length. Average cycle coefficient of friction was calculated from bi-
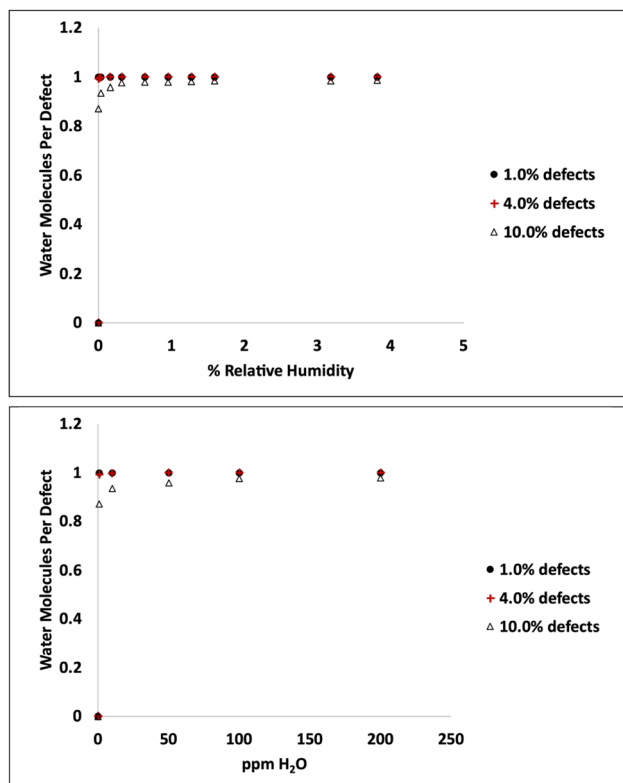
Fig. 2 Amount of water adsorbed per defect (S vacancy) at 298 K and low humidity levels.

directional friction loops using the methods of Burris and Sawyer.[49] The averages and standard deviations at each pressure are from the last 100 sliding cycles (steady-state region) of each experiment.

3 Results and discussion

3.1 Adsorption Isotherms for bulk MoS$_2$

Adsorption isotherms from GCMC simulations are shown in Fig. 1 for defect levels (sulfur vacancies) ranging from 0 to 10% of S atoms removed. 1% S defects corresponds to about 2.3×10^{13} defects per cm^2 and this is similar to the density of native point defects in MoS$_2$ monolayers grown by chemical vapor deposition.[50] Simulations indicate there is virtually no water adsorbed on defect-free MoS$_2$. In almost all cases with defects, the isotherms reach saturation at very low humidity levels. In a system with 1% S defects that has been exposed to humidity and saturated with water, about 0.25% of the mass of the system is water. This can have significant implications for applications highly sensitive to humidity. The same data is replotted in Fig. 2 where we show the amount of water adsorbed normalized by the number of defects. For 1% and 4% defects, the amount of water adsorbed corresponds to one water per S vacancy at humidities as low as 1 ppm water. For the case of 10% defects (2.3×10^{14} per cm^2), much higher than the typical amount in naturally MoS$_2$,[51,52] the isotherm does not reach saturation at low humidities, but the defects are

98% saturated at 1% RH. We note that the error bars for Fig. 1 and 2 are very small, essentially zero. The water binds to the defects sites and remains with no fluctuations. Raw data with error estimates for all GCMC simulations are given in the ESI.† Notably, the system with 10% defects never fully reaches 1.0 water molecule per defect site and only reaches a maximum of 99.5% saturation (we consider saturation to be 1 water molecule per defect site). We attribute this to a significant number of the defects being adjacent; in these cases the addition of water to a neighboring defect site is slightly less favored than adding a water to a single site because of the smaller charges. The charge on Mo on a single S vacancy is around 0.58 compared to 0.7 with no defect. For an Mo atom missing two S ligands, however, the partial charge is reduced to about 0.3–0.4, weakening the attractive force. This is consistent with results from DFT calculations in our previous work.[37] It is interesting to note that the S–S distance on MoS$_2$ is $\sim$3.15 Å, which is close to the average water–water separation distance in liquid water at ambient conditions (3.1 Å). Therefore, we can surmise water should fit into the S vacancy site, and when two water molecules are bound to adjacent sites, their respective spacing is close to that of liquid water.

3.2 MoS$_2$ surfaces

As we are primarily interested in the effects of water on the tribology of MoS$_2$ (i.e., surface properties), we also simulated water adsorption onto S vacancies on the surface of MoS$_2$. This system consists of three layers of MoS$_2$ with 20 Å of vacuum space above the top layer, as shown in Fig. 3B, with 0 to 5 defects on the basal surface. For the structures with 0 to 3 defects, the defects are placed randomly, but specifically not adjacent to other defects. As the density of defects increases, adjacent defects become statistically more likely, so we consider the effects of adjacent defect sites. For the structures with 4 and 5 defects, two structures were created, one without adjacent defects, and one with two adjacent defects (e.g., 2 adjacent and 3 isolated for a total of 5 defects). Visualizations of the structures are shown in ESI Fig. 3.†

As in bulk MoS$_2$, we find that the defects are saturated by water molecules at very low humidity levels (Fig. 3C). Again, no water is adsorbed on the defect-free surface. As the humidity increases, small clusters of water nucleate on the defect sites increasing the ratio of water to defects (Fig. 3D) up to about 1.4–1.8 water molecules per defect. Notably, the surfaces with adjacent defect sites adsorb more water than those with only isolated sites. This might seem to contradict our previous conclusion from Fig. 2 that adjacent defect sites are less favorable for adsorption. That conclusion, however, only applies to the *first* water molecule that binds to the S vacancy. Subsequent water molecules bind to the initial water *via* hydrogen bonding, and these additional molecules prefer sites with two adjacent water molecules to form two hydrogen bonds (Fig. 4). Therefore, adjacent defect sites *decrease* the affinity of the MoS$_2$ surface for a single water molecule because of the reduced Coulomb attraction, but adjacent sites with previously bound water molecules *increase* the binding affinity for a second layer of water due to increased hydrogen bonding.
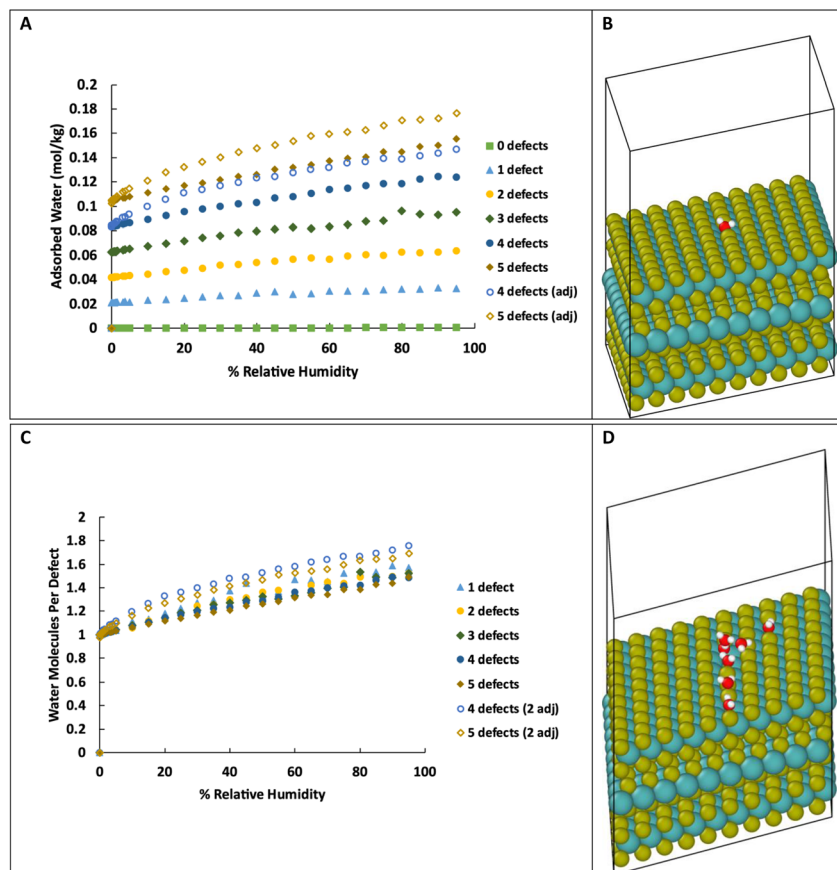
Fig. 3 (A) Adsorption isotherms for water on the surface of MoS_2 with different numbers of defects. Units are moles of water adsorbed per kg of MoS_2. (B) Visualization of a MoS_2 surface with one defect site and one water molecule adsorbed to the defect. (C) Amount of water adsorbed per defect site on the MoS_2 surface. The series denoted with "2 adj" have adjacent defect sites. (D) Visualization of a MoS_2 surface with 4 defect sites with small water clusters forming. Color key: O red, H white, S gold, Mo teal. Temperature is 298 K for all figures. System size: $31.475 \times 31.475 \times 35.0$ Å.
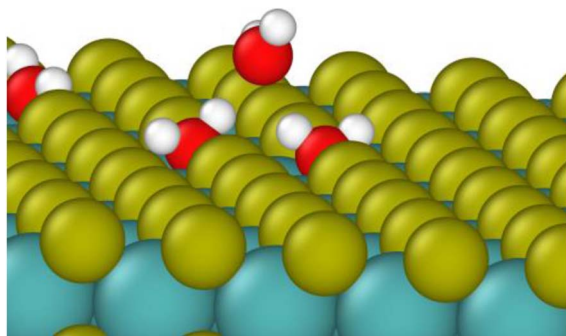

Fig. 4 Water molecule stabilized on a defect site by two hydrogen bonds. Colors: red O, white H, yellow S, teal Mo.

For the surface with 5 defects, at the lowest humidity (0.003% RH, 298 K), the structure with adjacent defects contains an average 0.98 water molecules per defect while the structure with non-adjacent defects is completely saturated with 1 water per defect. This is in agreement with the results of simulations in bulk with high defect density. However, at 90%

RH, the structure with adjacent defects has 1.65 water molecules per defect, compared to 1.43 for the non-adjacent defects.

The breakdown of the adsorption energy into the van der Waals and Coulomb energy contributions is shown in Fig. 5. Note these values are the total energy of adsorbate–adsorbate or adsorbate–MoS_2 interactions, including O_2, N_2, and Ar. There are no Mo–S interactions included. However, as very little of the other atmospheric species are adsorbed on the MoS_2 in the GCMC simulations, the energies shown are almost entirely due to water.

Fig. 5A and C show the adsorbate–adsorbate and adsorbate–host (MoS_2) interactions in bulk MoS_2 with 1% defects, respectively, corresponding to the isotherms in Fig. 1. The energies mirror the adsorption isotherm in that they show no dependence on humidity; S vacancies are saturated with water at low humidities and no more water is adsorbed as humidity increases. Energetic interactions are dominated by water–MoS_2 Coulomb attraction, and the adsorbate–MoS_2 van der Waals interaction is slightly unfavorable, likely due to the water molecule being confined to a small volume around the defect. However, the strong Coulomb attraction overcomes this.
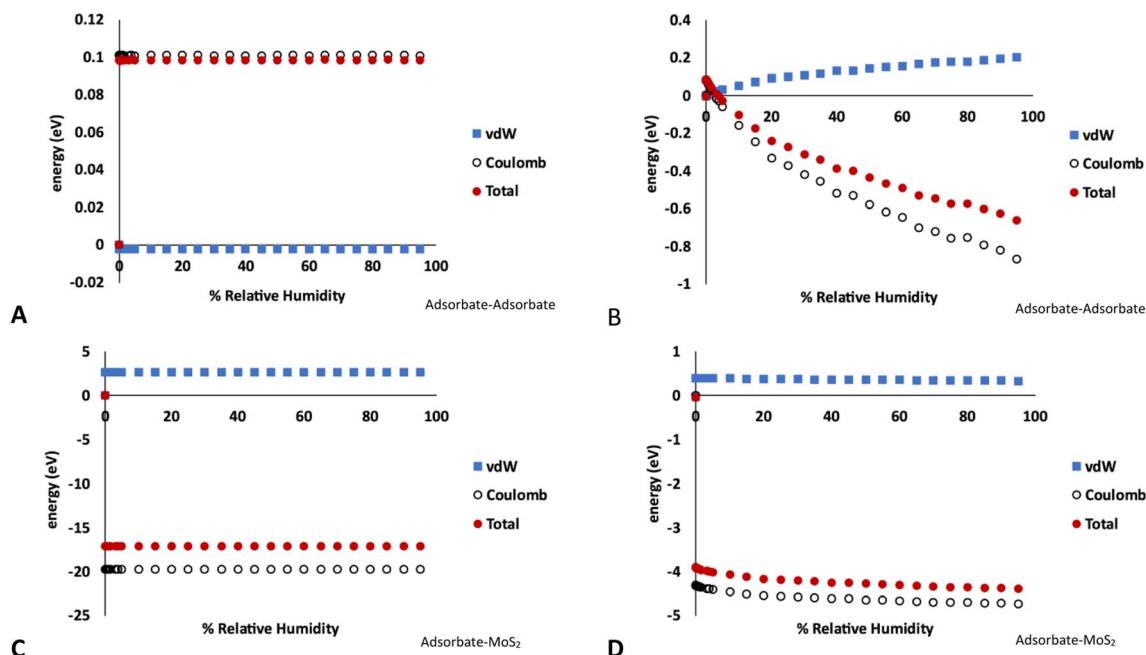
Fig. 5 Energy decomposition (energy units in eV) for water adsorption in MoS_2 at 298 K. These values represent the total energy of either adsorbate–adsorbate or adsorbate–host interactions in the simulation, averaged over the length of the GCMC simulation. (A) Adsorbate–adsorbate interactions in bulk MoS_2 (1% defects), (B) adsorbate–adsorbate interactions on MoS_2 surface (4% defects), (C) adsorbate–MoS_2 interactions in bulk MoS_2 (1% defects), (D) adsorbate–MoS_2 interactions on MoS_2 surface (4% defects). Note the different energy scales in A–D. Raw data with error bars is given in the ESI.†

Table 1 Mole fraction of gases (excluding water) adsorbed to MoS_2 surface. Gas phase indicates the mole fraction of components in the GCMC reservoir which approximates dry atmosphere

Defects	0	1	2	3	4	Gas phase
O_2	0.22	0.21	0.21	0.21	0.21	0.21
N_2	0.77	0.78	0.78	0.78	0.77	0.78
Ar	0.01	0.01	0.01	0.01	0.01	0.01

In the case of water adsorption on the surface at 298 K and 4% defects (Fig. 5B and D, corresponding to the isotherms shown in Fig. 3A), the adsorbate–host interactions are essentially independent of humidity, similar to the bulk case. However, the adsorbate–adsorbate interaction energy become much more strongly negative as humidity increases, indicating stronger water–water interactions. As above, the interactions are dominated by Coulomb attraction. It is clear from this figure that the surface defects are saturated by water molecules at low humidity, and as the humidity increases more water molecules bind *via* hydrogen bonding to form clusters on the surface.

3.3 Other gases

In general, we find very little O_2, N_2, or Ar adsorbed on the MoS_2 surface. As with water, there is not enough space between the layers in the bulk to adsorb gas molecules, but they can bind to the surface. GCMC simulations indicate that a small amount of these gases is adsorbed, but in the same proportion as they are

present in the atmosphere. This indicates MoS_2 has no selectivity towards Ar, O_2 or N_2. As shown in Table 1, the presence of defects does not change this behavior, and defects do not impart any selectivity or significantly increase the amount of O_2, N_2, and Ar adsorbed. This is because the water out-competes the atmospheric gases for binding sites on the defects, and makes sense in light of the data shown in Fig. 5 that indicates that water adsorption is largely driven by Coulomb interactions; O_2, N_2, and Ar are all nonpolar molecules. At 298 K and 50% RH (on a surface with a single defect) the adsorption enthalpy for water is −37.5 kJ mol^{-1}, compared to −6.3, −6.6, and −6.6 kJ mol^{-1} for N_2, O_2, and Ar respectively (computed by RASPA during GCMC simulation). Therefore, defect sites are much more likely to contain a water molecule that will not be dislodged by O_2 or N_2.

3.4 Effects of layer separation

The GCMC simulations indicate that at their crystallographic minimum, the MoS_2 lamellae are too close together to permit more than one water molecule per defect to adsorb. However, in these simulations the MoS_2 is held fixed while our previous work indicated that water adsorption can disrupt the MoS_2 crystal structure by causing layers to separate.[37] As there is a significant energetic penalty for this separation, the question arises how far apart must layers be pushed in order to permit more water adsorption. To study this effect, we performed a series of simulations with four layers of MoS_2 with the interlayer distance ranging from the minimum (Mo–Mo distance
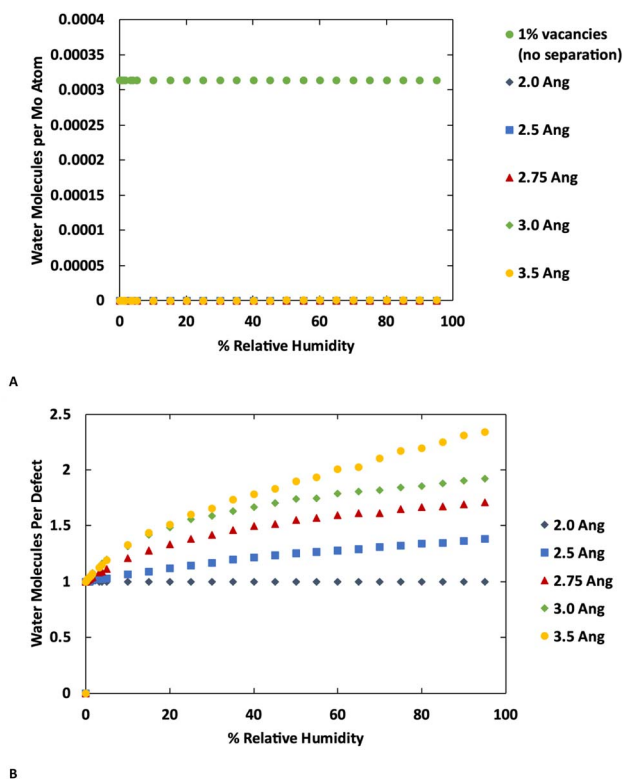
Fig. 6 Adsorption isotherms for water at 298 K in MoS_2 with lamellae separation increased from the ideal distance by 2.0, 2.5, 2.75, 3.0, and 3.5 Å. (A) shows the isotherms normalized as water per Mo atom for defect-free MoS_2 compared to MoS_2 with 1% defects (B) shows the isotherms normalized as water per defect for MoS_2 with 1% random S vacancy defects.

6.3 Å) to an additional 3.5 Å of separation. The results are shown in Fig. 6 (also ESI Fig. 7 and ESI Fig. 8†) for MoS_2 with and without defects.

No additional water is adsorbed with up to 2.0 Å of additional separation. At 2.5 Å a very small amount of extra water adsorbs in the defect-free MoS_2, while more significant amounts of extra water are adsorbed at 3.0 Å or greater separations. Water is primarily adsorbed to the defect sites or small clusters of water around the defects. These results are consistent with the kinetic diameter of water of 2.65 Å.[53] In the defective MoS_2, as before, there is no additional water adsorbed with only 2.0 Å of increased separation, but further separation leads to more water adsorption.

Interestingly we find that the isotherm shape is different in the defect-free and defective MoS_2. In the defect-free system, the isotherm is linear with humidity (pressure) indicating Henry behavior, with the Henry coefficient increasing with layer separation distance. This is due to the uniformity of the MoS_2 without defects where there is no differentiation among binding sites. In the defective MoS_2, however, the isotherm takes on a classic Type I Langmuir shape, consistent with adsorption in porous materials like zeolites. This indicates a stronger interaction with the MoS_2 defect sites, while the

pristine MoS_2 is largely hydrophobic as shown in Fig. 6A (also Fig. 1 and 3). Notably, for bulk MoS_2 with defects (Fig. 1) the isotherm is essentially flat because it saturates at very low humidity. This could be viewed as a Type I isotherm with very high interaction strength, as seen in the 10% defects case.

Separating the layers of MoS_2 from their normal minimum position requires energy. Alternatively, one can think of this value as the amount of energy driving MoS_2 lamellae to return to their optimal position and effectively push out adsorbates like water.[54,55] This is important for tribological applications where water is likely entrained in the bulk of MoS_2 but eventually diffuses out.[29,56,57]

To determine how much energy is associated with MoS_2 layer separation, we used DFT calculations (PBE functional, 520 eV, DFT details same as our previous work[37]) on a 5×5 unit cell of MoS_2 with 4 layers in the 2H configuration (ESI Fig. 2†). Starting with the minimized geometry, we increased the distance between two layers (leaving the others unchanged) up to 10 Å of separation beyond the crystallographic minimum. At this point, the energy no longer changes with increasing separation, indicating that the two layers are no longer interacting. This was repeated for MoS_2 structures with one S vacancy on the surface of one of the separated layers, two adjacent S vacancies on the surface of a separated layer, and two S vacancies on opposing layers (on the site of the nearest neighbor S directly above the first defect). The data in Fig. 7 show only minor differences between these two configurations. The energy of separating layers with two adjacent defects is slightly lower at large distances.

More significantly, the energy of separating defective layers is *higher* than pristine MoS_2 at small distances up to ~0.5 Å, indicating that they are more difficult to separate than pristine MoS_2. At 0.75 Å or greater, this trend changes and defective MoS_2 becomes easier to separate. At the smaller distances (<0.5 Å), the defective layers bind to each other more tightly due to attraction between unsaturated defect sites. We attribute this to electronic communication between the unsaturated states at defects on the lamellae at the closer distance. At 10 Å, the difference between defect-free structure and that with one defect is about 0.06 eV nm^{-2} compared to 0.1–0.11 eV nm^{-2} for two defects. At this distance we attribute this difference mostly to weaker dispersion interactions from the missing atoms, which reduces the number of pairwise interactions in the system.

3.5 Defects on edges

To this point we have focused on defects on the basal surface. However, defects on the edges of MoS_2 lamellae have a strong influence over tribological properties.[35,36] Therefore, we next consider water adsorption to edges of MoS_2 with and without S defects. This was done by removing a stoichiometric slice of a layer, creating a small cavity, followed by the removal of random S atoms along the edges to create defects. This is meant to mimic gaps between sheets or flakes of MoS_2 deep in the bulk, as was shown in our previous work to impact tribological performance. The simulation box was duplicated to ensure the
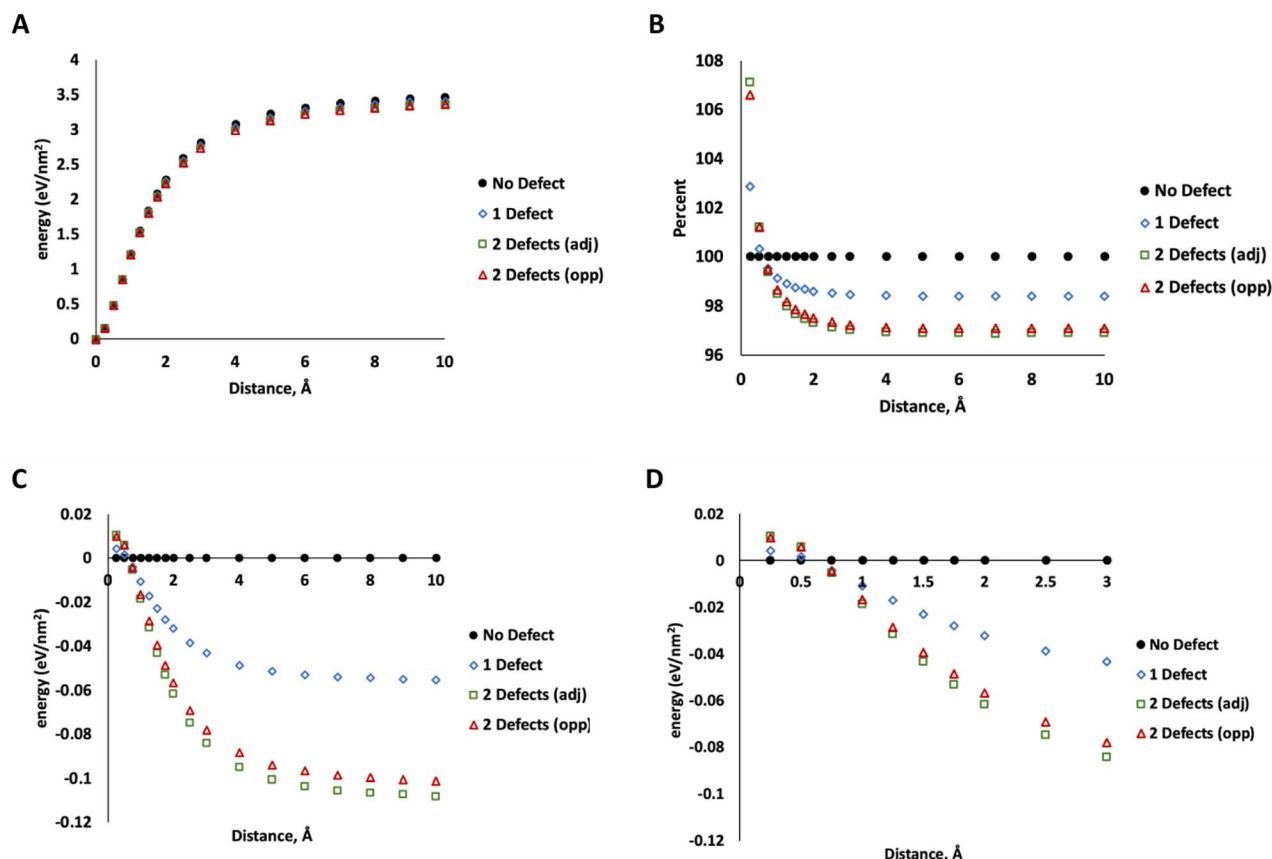
Fig. 7 (A) Energy per nm^2 required to pull apart two MoS_2 lamellae to a distance given on the horizontal axis. Energy is represented as the difference from the minimum. (B) Difference in the energy of displacing defect-free and defective MoS_2, relative to the energy of the defect-free system at each point, expressed as a percentage of the defect-free case at each step. 100% represents the energy of the defect-free structure at the minimum position (C) difference in the energy of displacing defect-free and defective MoS_2, relative to the energy of the defect-free system at each point, expressed in $eV\ nm^{-2}$. (D) Same as C with horizontal axis zoomed in for clarity.

length of the simulation box in the Z direction was greater than twice the Lennard-Jones cutoff (shown in Fig. 8B).

Results of the GCMC simulations with edge defects at 298 K are shown in Fig. 8 (278 K and 313 K) are shown in ESI Fig. 6.† As with the basal surfaces, very little water adsorbs on the edge when no defects are present. However, more water adsorbs to the defect-free edges compared to the defect-free surface or bulk (0.00033 mol kg^{-1} on surface *vs.* 0.0028 mol kg^{-1} on edges at 298 K, 80% RH, 0 mol kg^{-1} in defect free bulk) When defects are present on the edges, they are saturated with one water molecule per vacancy at low relative humidity. From that point, the amount of water adsorbed increases nearly linearly with humidity. In the case of 25% edge defects (10 of the 40 edge S removed) we see Type IV isotherm behavior around 80–95% humidity as the water clusters around the defect sites and begins to exhibit capillary condensation. Note that this defect level is similar to that in our previous work with stoichiometric MoS_2 nanoplatelets.[35,36] In that work, perfectly terminated flakes were highly non-stoichiometric (with excess S), but stoichiometric flakes had ~30% defects in the form of removed S atoms along the edges.

Notably, although the edge defects are mostly saturated with water at low humidity, the humidity level for saturation is not as low as in the case of the basal surface defects (Fig. 1), which are saturated almost immediately. The system with 12.5% defects does not reach 1 water molecule per defect site until 3% humidity (around 940 ppm at 298 K), which is practically quite low, but also markedly more than the structure with 4% defects on the basal surface that reached saturation at lower than 10 ppm water (0.03% RH). However, we note that all these saturation humidity levels are realistically quite low. For example, desert climates typically have relative humidities of 10–20%, and at these levels our results indicate that all defect sites in MoS_2 will be fully saturated.

The reason for this is not immediately clear from looking at the partial charges on the MoS_2 structure, as calculated *via* EQeq in RASPA.[45] In pristine MoS_2, Mo carries a charge of about 0.70 and S has a charge of −0.35. For a S vacancy on the surface, the Mo charge is reduced to 0.58. For an edge vacancy, the charge on the undercoordinated Mo is only reduced slightly to 0.68. Since we have determined previously that water adsorption is primarily driven by Coulomb interactions, it appears that
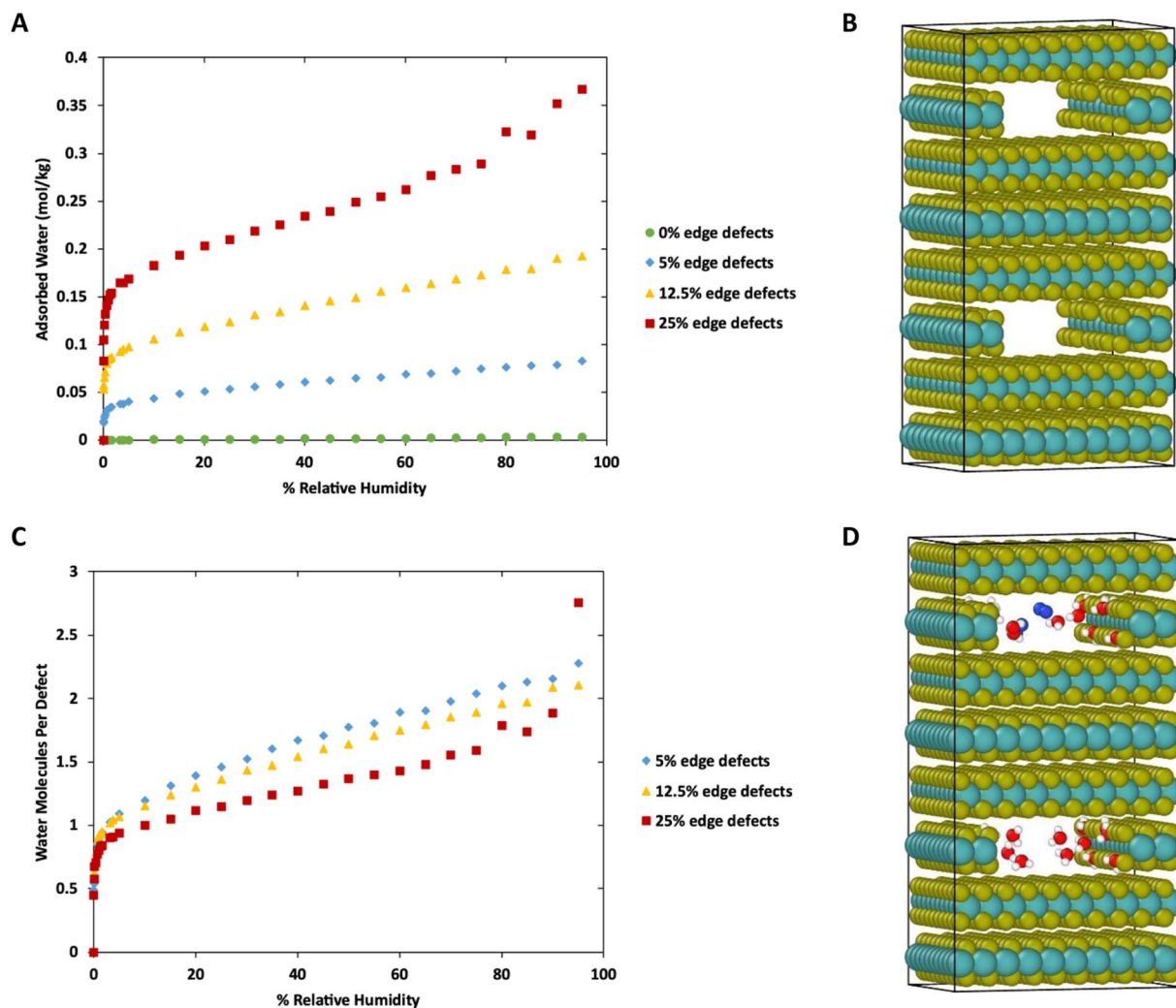
Fig. 8 (A) Adsorption isotherms in mol kg^{-1} for water in MoS$_2$ with edge defects. Temperature is 298 K. (B) Visualization of MoS$_2$ structure with edge defects. (C) Adsorption isotherms in water per defect site at 298 K. (D) Visualization of water adsorbed onto MoS$_2$ at 298 K and 90% RH. Colors: yellow S, teal Mo, red O, white H, blue N. System size: 31.475 × 31.475 × 48.288 Å.

the water should prefer to bind to the edge site with a stronger positive charge. However, the opposite is true.

To understand the binding to edge defects, it is useful to closely examine the binding positions of water on each type of defect, shown in Fig. 9. For the surface defect (Fig. 9A), the water occupies the vacancy left by the S, in close proximity to three Mo atoms (distances 2.5, 2.6, and 2.7 Å) while for the edge defects each water mostly interacts with only two Mo atoms (distances 2.5 and 2.7 Å). Therefore, despite the ostensibly weaker Coulomb attraction from Mo atoms on the surface, the addition of a third Mo increases the overall binding strength, resulting in more favorable binding on the surface.

Fig. 10 shows a comparison of water adsorption on bulk MoS$_2$, the basal surface of MoS$_2$, and the edges at 298 K. The surface and edge structures have 5% defects on the surface or edge, respectively, and no defects elsewhere. The bulk MoS$_2$ has defects on the basal surfaces. For the edge case, defects are only on the edge and there are no defects on the surface. For the

surface structure, there are five defects and none of them are adjacent (ESI Fig. 3F†). As expected from the results in Fig. 2, in bulk MoS$_2$, each defect adsorbs one water molecule. On the surface, the defects are saturated with one water molecule per site at very low humidity, and then the average number of water molecules per defect site increases linearly up to about 1.5 water molecules per defect at 95% humidity. For the edge defects case, at very low humidity (1 ppm water) the edges have an average 0.5 water molecules per defect site. The edge sites reach saturation at about 2.9% RH (314 ppm water) and the number of water molecules increases to 2.3 per defect at 95% RH. Notably, the isotherm also takes on a more typical Type I Langmuir shape.

We can see from Fig. 10 that at extremely low (<942 ppm or 3% RH at 298 K) levels of humidity, water favors binding to the basal surface or bulk, but at higher (>3%) levels of humidity the edge sites are preferred. This threshold is important because previous research indicates that water binding to edge defects
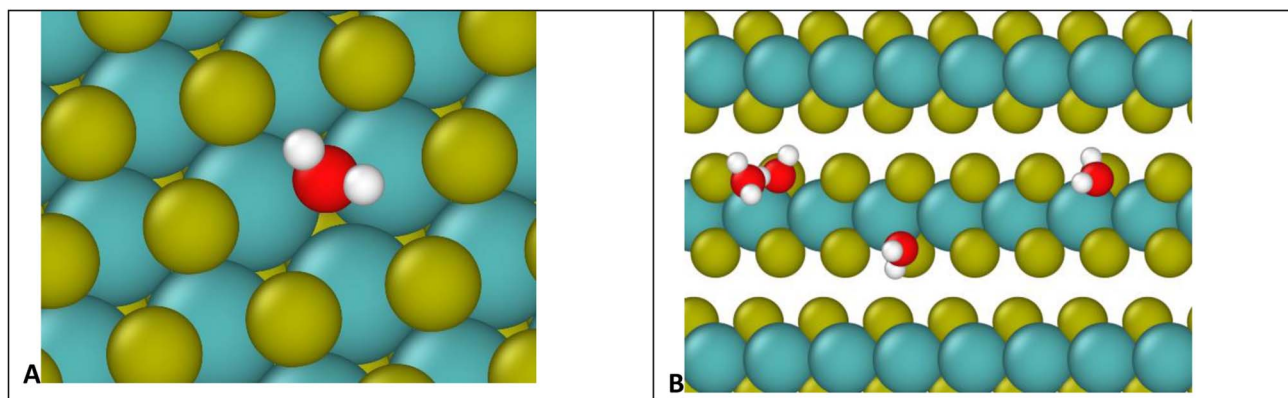
Fig. 9 Visualization of water molecules adsorbed to (A) defect on basal surface, (B) defects on an edge. Colors: yellow S, red O, white H, teal Mo. The relative sizes of the atoms are for clarity, and do not represent reality.

impact the tribological performance,[36] and these results agree with experimental values (Section 3.6). At higher humidity, the water molecules in excess of one water molecule per defect site are largely adsorbed *via* hydrogen bonding to water molecules that are already bound to the surface. The hydrogen bonding should not be impacted by the location of the S defects (edge *vs.* surface), so it is interesting that the edge sites attract more water. We attribute this to the additional van der Waals attraction from the layers above and below the edge site, creating a small pore.

The structures in Fig. 10 each have defects in only one location. However, real MoS_2 systems will have a distribution of defects across both surface and edge sites. To better model real systems, we repeated the calculations on a structure that contains an edge and basal surface, with 1% defects randomly distributed throughout the structure (Fig. 11A). In this case, there are 7 total defects: 1 on the edge and 6 on the surfaces. Based on the previous results in Fig. 1 and 2, we can assume the surface defects that are in the bulk will each adsorb only one water molecule, and the rest of the water in the system will be adsorbed on the edge defects. Using this assumption, we see in Fig. 11B similar behavior to the individual structures in Fig. 10. At low humidity the edge defects are not

Fig. 10 Water adsorption isotherms at 298 K for MoS_2 surface, bulks MoS_2, and MoS_2 edges. All structures contain 5% defects on only the surface or edge, as indicated in the legend.

saturated, until about 5% RH in this case. At 95% RH the edge defects adsorb a little over 2 water molecules per site on average. The heat of adsorption (Fig. 11C) is about -62 kJ mol^{-1} at low humidity and then around -37 kJ mol^{-1} at high humidity. This corresponds to water binding to the more favorable surface sites at the lowest humidity, followed by the edge sites, and then a second layer of water binding to adsorbed water molecules on edge sites *via* hydrogen bonding.

3.6 Implications for tribology

Based on our simulations, it is clear that any defect sites in MoS_2 will be nearly saturated with water even at humidity levels as low as 3% relative humidity (around 940 ppm at 298 K). This implies that any exposure to humid atmosphere during synthesis, processing or testing will certainly result in significant quantities of water adsorption, depending on the defect density. For 1% defects at 298 K, this could be around 0.2 wt% water or greater in the MoS_2.

Based on results in Fig. 11, after the surface defects are saturated, most of the adsorbed water will bind to defects on edge sites, where it will disrupt formation of larger lamellae and inhibit the effectiveness of the lubricant.[36] These results agree with previous work that demonstrated water's ability to coalesce at edges of MoS_2 lamellae, preventing formation of larger lamellae leading to higher friction coefficients. Friction tests as a function of the partial pressure of water in the atmosphere (Fig. 12) corroborate these results, showing a distinct increase in friction coefficient around 0.15–1.0 torr, or approximately 130–1300 ppm water. This suggests that the saturation of water at edges of MoS_2 lamellae lead to the increase in friction observed in dynamic sliding and prevent lubrication by inhibiting formation of long term ordered surface lamellae. This agrees with the simulations that indicate that surface or bulk defects saturate first, around 3% relative humidity (940 ppm, 0.7 torr), and then water starts binding to the edges where it impacts tribological performance. As described in our previous work[36] water bound to the edges of small MoS_2 flakes will inhibit the formation of larger lamellae that are responsible for the low friction
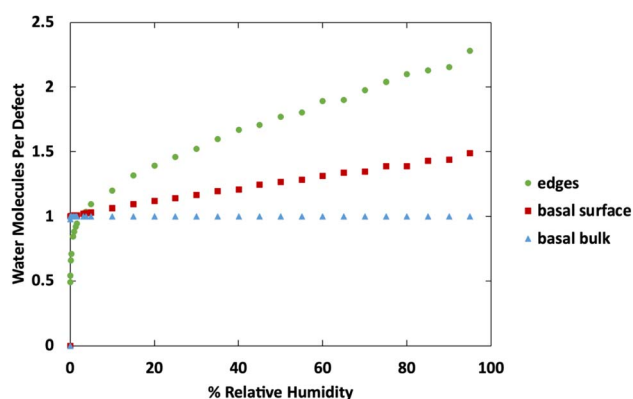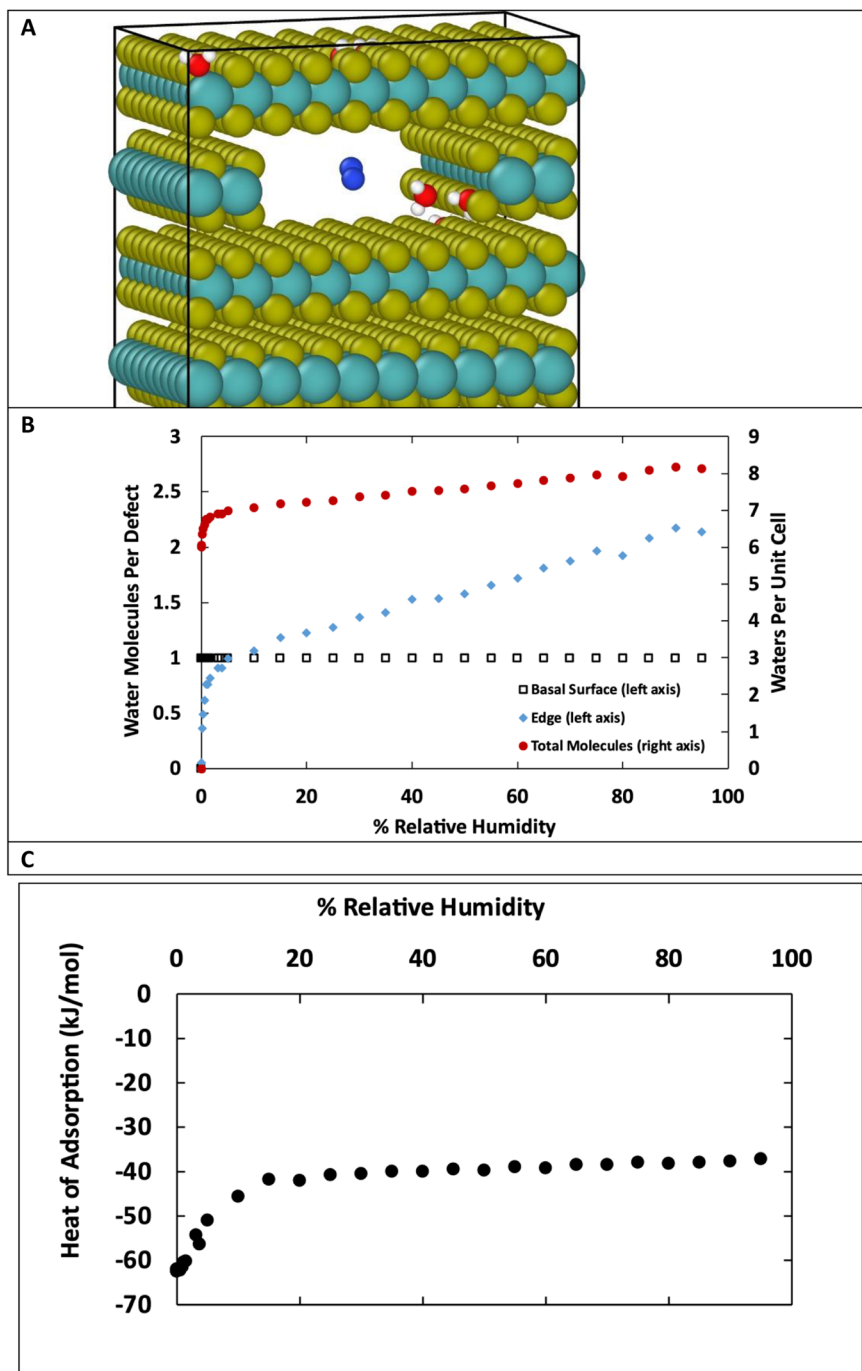
Fig. 11 (A) Snapshot from GCMC simulation in MoS_2 with 1% defects, including edge and surface defects. Colors: yellow S, teal Mo, red O, white H, blue N. (B) Adsorption isotherm for water at 298 K on MoS_2 structure containing both basal surface and edge defects. This structure has 6 surface defects and 1 edge defect, for 7 total defects, representing 1% of the total S atoms. (C) Heat of adsorption of water in kJ mol^{-1}.

coefficient generally found in MoS_2. As shown in Fig. 12, small amounts of water (which simulations indicate are likely bound to the surface instead of the edges) do not impact tribological performance significantly.

We posit that it is a reasonably valid assumption that each surface vacancy (between the lamellae) will contain only one water, and all other water is mostly likely bound to edge sites

or condensed in micropores between the lamellae. We find that within the range of 278 K to 313 K, there is not a large effect of temperature on the amount of water adsorbed on MoS_2, (see ESI Fig. 4–ESI Fig. 6†), though there is slightly more water adsorbed at higher temperatures due to the higher humidity/vapor pressure.
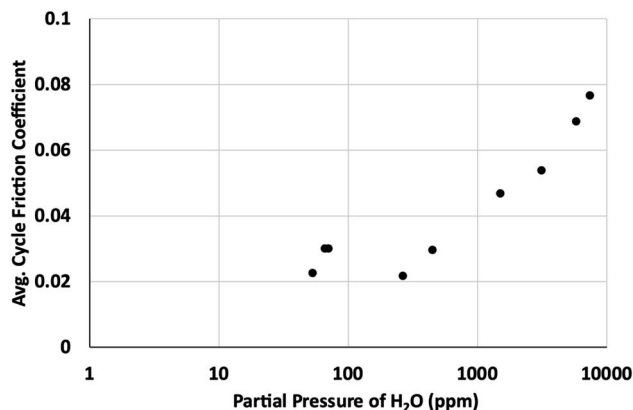
Fig. 12 Average cycle friction coefficient as a function of partial pressure of water in parts per million (ppm).

4   Conclusions

In this work we used GCMC simulations to systematically study water adsorption on MoS_2 with defects on surfaces and edges. Although it has been commonly known for a long time that water impacts the tribological performance of MoS_2, the mechanisms of water adsorption under exposure to realistic atmospheres have not been rigorously studied previously. We find that pristine MoS_2 is generally hydrophobic, and water adsorption is heavily influenced by defects. The adsorption mechanism is dominated by Coulomb attraction between water and positively charged Mo atoms at defects sites, and subsequently by hydrogen bonding between a second layer of water and the water molecules bound to the MoS_2. At a representative atmospheric condition of 298 K and 5% RH, MoS_2 with 1% defects (a realistic value for real MoS_2) can contain 0.2 wt% water or more. We find no significant adsorption of O_2, N_2, or argon.

Water preferentially binds to defects on the basal surface first due to geometric effects that allow interactions with three Mo atoms at once; however, these sites are saturated at low ppm humidity and in bulk MoS_2 can only hold one water per site. Water molecules bound to the surface or edges nucleate small clusters of water *via* hydrogen bonding. Ultimately, most water will go to defect sites on the edges, and our previous work has shown that water bound to edges of MoS_2 flakes play a critical role in the negative impact on tribology.[36]

We also used DFT to compute the energy of separating layers of MoS_2 to permit higher water adsorption. GCMC simulations indicate water will not intercalate the layers until they are separated at least 2.5 Å beyond their usual minimum position, and this requires about 2.5 eV nm^{-2}. Interestingly, the inclusion of defects increases the energy required to separate layers at small distances (<0.5 Å) but reduces it slightly at longer distances.

Generally, defect sites are completely saturated with water at very low (ppm) humidity. However, we find that MoS_2 with high defect density (10%) does not saturate at low humidity and never truly reaches 100% saturation (98% saturated at 1% RH

and higher). We attribute this to the presence of more adjacent defects that we show are slightly less favorable binding sites for water. However, adjacent defect sites on surfaces result in *more* water adsorption at medium or high humidities because water molecules bound to adjacent sites create ideal binding sites for a third water molecule stabilized by two hydrogen bonds.

While surface defects in bulk MoS_2 are more favorable for water adsorption than edges, edge sites also readily bind water and have more room for a second layer adsorbed to the bound water molecules. (In the bulk, each defect can contain only one water molecule.) Therefore, we conclude at very low humidity, surface defect sites are saturated, and at higher humidity (about 3% relative humidity) edge sites become saturated and take on more water. Water binding to the edge sites disrupts the formation of ordered surface lamellae and reduces the effectiveness of the lubricant.[29,36]

Practically, all defect sites are saturated above 3–5% relative humidity and virtually all MoS_2 that has been exposed to regular atmosphere should be considered saturated with at least one water molecule per defect site.

Conflicts of interest

There are no conflicts to declare.

Acknowledgements

References

1 U. Krishnan, M. Kaur, K. Singh, M. Kumar and A. Kumar, A Synoptic Review of MoS_2: Synthesis to Applications, *Superlattices Microstruct.*, 2019, **128**, 274–297.

2 X. Li and H. Zhu, Two-Dimensional MoS_2: Properties, Preparation, and Applications, *J. Materiomics*, 2015, **1**, 33–44.

3 J. Sun, X. Li, W. Guo, M. Zhao, X. Fan, Y. Dong, C. Xu, J. Deng and Y. Fu, Synthesis Methods of Two-Dimensional MoS_2: A Brief Review, *Crystals*, 2017, **7**, 198.

4 L. S. Byskov, J. K. Nørskov, B. S. Clausen and H. Topsøe, Edge Termination of MoS₂ and Comos Catalyst Particles, *Catal. Lett.*, 2000, **64**, 95–99.

5 Y. Cao, Roadmap and Direction toward High-Performance MoS₂ Hydrogen Evolution Catalysts, *ACS Nano*, 2021, **15**, 11014–11039.

6 L. Lei, D. Huang, G. Zeng, M. Cheng, D. Jiang, C. Zhou, S. Chen and W. Wang, A Fantastic Two-Dimensional MoS₂ Material Based on the Inert Basal Planes Activation: Electronic Structure, Synthesis Strategies, Catalytic Active Sites, Catalytic and Electronics Properties, *Coord. Chem. Rev.*, 2019, **399**, 213020.

7 S. Singh, A. Modak, K. K. Pant, A. Sinhamahapatra and P. Biswas, MoS₂–Nanosheets-Based Catalysts for Photocatalytic CO₂ Reduction: A Review, *ACS Appl. Nano Mater.*, 2021, **4**, 8644–8667.

8 J. Mao, Y. Wang, Z. Zheng and D. Deng, The Rise of Two-Dimensional Mos₂ for Catalysis, *Front. Phys.*, 2018, **13**, 138118.

9 M. Donarelli and L. Ottaviano, 2d Materials for Gas Sensing Applications: A Review on Graphene Oxide, MoS₂, Ws₂ and Phosphorene, *Sensors*, 2018, **18**, 3638.

10 O. Samy, S. Zeng, M. D. Birowosuto and A. El Moutaouakil, A Review on MoS₂ Properties, Synthesis, Sensing Applications and Challenges, *Crystals*, 2021, **11**, 355.

11 R. Kumar, W. Zheng, X. Liu, J. Zhang and M. Kumar, MoS₂-Based Nanomaterials for Room-Temperature Gas Sensors, *Adv. Mater. Technol.*, 2020, **5**, 1901062.

12 O. V. Yazyev and A. Kis, MoS₂ and Semiconductors in the Flatland, *Mater. Today*, 2015, **18**, 20–30.

13 E. Singh, P. Singh, K. S. Kim, G. Y. Yeom and H. S. Nalwa, Flexible Molybdenum Disulfide (MoS₂) Atomic Layers for Wearable Electronics and Optoelectronics, *ACS Appl. Mater. Interfaces*, 2019, **11**, 11061–11105.

14 Y. Chen, S. Huang, X. Ji, K. Adepalli, K. Yin, X. Ling, X. Wang, J. Xue, M. Dresselhaus and J. Kong, Tuning Electronic Structure of Single Layer MoS₂ through Defect and Interface Engineering, *ACS Nano*, 2018, **12**, 2569–2579.

15 I. D. Marion, D. Čapeta, B. Pielić, F. Faraguna, A. Gallardo, P. Pou, B. Biel, N. Vujičić and M. Kralj, Atomic-Scale Defects and Electronic Properties of a Transferred Synthesized MoS₂ Monolayer, *Nanotechnology*, 2018, **29**, 305703.

16 K. Santosh, R. C. Longo, R. Addou, R. M. Wallace and K. Cho, Impact of Intrinsic Atomic Defects on the Electronic Structure of MoS₂ Monolayers, *Nanotechnology*, 2014, **25**, 375703.

17 M. R. Vazirisereshk, A. Martini, D. A. Strubbe and M. Z. Baykara, Solid Lubrication with MoS₂: A Review, *Lubricants*, 2019, **7**, 57.

18 A. Savan, E. Pflüger, P. Voumard, A. Schröer and M. Simmonds, Modern Solid Lubrication: Recent Developments and Applications of MoS₂, *Lubric. Sci.*, 2000, **12**, 185–203.

19 M. Bell and J. Findlay, Molybdenite as a New Lubricant, *Phys. Rev.*, 1941, **59**, 922.

20 K. P. Furlan, J. D. B. de Mello and A. N. Klein, Self-Lubricating Composites Containing MoS₂: A Review, *Tribol. Int.*, 2018, **120**, 280–298.

21 T. Spalvins, A Review of Recent Advances in Solid Film Lubrication, *J. Vac. Sci. Technol., A*, 1987, **5**, 212–219.

22 Y. Xu, K. Fu, K. Liu, K. Sun, Y. Dong and L. Yao, A State of the Art Review of the Tribology of Graphene/MoS₂ Nanocomposites, *Mater. Today Commun.*, 2022, 105108.

23 S. H. Mukhtar, M. Wani, R. Sehgal and M. Sharma, Nano-Mechanical and Nano-Tribological Characterisation of Self-Lubricating MoS₂ Nano-Structured Coating for Space Applications, *Tribol. Int.*, 2023, **178**, 108017.

24 J. Gao, B. Li, J. Tan, P. Chow, T.-M. Lu and N. Koratkar, Aging of Transition Metal Dichalcogenide Monolayers, *ACS Nano*, 2016, **10**, 2628–2635.

25 P. Budania, P. Baine, J. Montgomery, C. McGeough, T. Cafolla, M. Modreanu, D. McNeill, N. Mitchell, G. Hughes and P. Hurley, Long-Term Stability of Mechanically Exfoliated MoS₂ Flakes, *MRS Commun.*, 2017, **7**, 813–818.

26 T. N. Walter, F. Kwok, H. Simchi, H. M. Aldosari and S. E. Mohney, Oxidation and Oxidative Vapor-Phase Etching of Few-Layer MoS₂, *J. Vac. Sci. Technol. B*, 2017, **35**, 021203.

27 T. Liang, W. G. Sawyer, S. S. Perry, S. B. Sinnott and S. R. Phillpot, Energetics of Oxidation in MoS₂ Nanoparticles by Density Functional Theory, *J. Phys. Chem.*, 2011, **115**, 10606–10616.

28 T. Liang, W. G. Sawyer, S. S. Perry, S. B. Sinnott and S. R. Phillpot, First-Principles Determination of Static Potential Energy Surfaces for Atomic Friction in MoS₂ and MoO₃, *Phys. Rev. B*, 2008, **77**, 104105.

29 H. Khare and D. Burris, Surface and Subsurface Contributions of Oxidation and Moisture to Room Temperature Friction of Molybdenum Disulfide, *Tribol. Lett.*, 2014, **53**, 329–336.

30 M. Stella, C. D. Lorenz and M. C. Righi, Effects of Intercalated Water on the Lubricity of Sliding Layers under Load: A Theoretical Investigation on MoS₂, *2D Mater.*, 2021, **8**, 035052.

31 J. Panitz, L. Pope, J. Lyons and D. Staley, The Tribological Properties of MoS₂ Coatings in Vacuum, Low Relative Humidity, and High Relative Humidity Environments, *J. Vac. Sci. Technol., A*, 1988, **6**, 1166–1170.

32 V. E. P. Claerbout, P. Nicolini and T. Polcar, Exploring Nanoscale Lubrication Mechanisms of Multilayer MoS₂ During Sliding: The Effect of Humidity, *Front. Chem.*, 2021, **9**, 450.

33 E. Serpini, A. Rota, A. Ballestrazzi, D. Marchetto, E. Gualtieri and S. Valeri, The Role of Humidity and Oxygen on MoS₂ Thin Films Deposited by RF Pvd Magnetron Sputtering, *Surf. Coat. Technol.*, 2017, **319**, 345–352.

34 J. F. Curry, N. Argibay, T. Babuska, B. Nation, A. Martini, N. C. Strandwitz, M. T. Dugger and B. A. Krick, Highly Oriented Mos₂ Coatings: Tribology and Environmental Stability, *Tribol. Lett.*, 2016, **64**, 1–9.

35 J. F. Curry, M. A. Wilson, H. S. Luftman, N. C. Strandwitz, N. Argibay, M. Chandross, M. A. Sidebottom and B. A. Krick, Impact of Microstructure on MoS$_2$ Oxidation and Friction, *ACS Appl. Mater. Interfaces*, 2017, **9**, 28019–28026.

36 J. F. Curry, T. Ohta, F. W. DelRio, P. Mantos, M. R. Jones, T. F. Babuska, N. S. Bobbitt, N. Argibay, B. A. Krick and M. T. Dugger, Structurally Driven Environmental Degradation of Friction in MoS$_2$ Films, *Tribol. Lett.*, 2021, **69**, 1–10.

37 N. S. Bobbitt and M. Chandross, Interactions of Water with Pristine and Defective MoS$_2$, *Langmuir*, 2022, **38**, 10419–10429.

38 R. Holinski and J. Gänsheimer, A Study of the Lubricating Mechanism of Molybdenum Disulfide, *Wear*, 1972, **19**, 329–342.

39 X. Zhao, G. Zhang, L. Wang and Q. Xue, The Tribological Mechanism of MoS$_2$ Film under Different Humidity, *Tribol. Lett.*, 2017, **65**, 1–8.

40 M. Uemura, K. Saito and K. Nakao, A Mechanism of Vapor Effect on Friction Coefficient of Molybdenum Disulfide, *Tribol. Trans.*, 1990, **33**, 551–556.

41 R. Addou, L. Colombo and R. M. Wallace, Surface Defects on Natural MoS$_2$, *ACS Appl. Mater. Interfaces*, 2015, **7**, 11921–11929.

42 D. Dubbeldam, S. Calero, D. E. Ellis and R. Q. Snurr, Raspa: Molecular Simulation Software for Adsorption and Diffusion in Flexible Nanoporous Materials, *Mol. Simul.*, 2016, **42**, 81–101.

43 Z. Gu, P. De Luna, Z. Yang and R. Zhou, Structural Influence of Proteins Upon Adsorption to MoS$_2$ Nanomaterials: Comparison of MoS$_2$ Force Field Parameters, *Phys. Chem. Chem. Phys.*, 2017, **19**, 3039–3045.

44 W. L. Jorgensen, J. Chandrasekhar, J. D. Madura, R. W. Impey and M. L. Klein, Comparison of Simple Potential Functions for Simulating Liquid Water, *J. Chem. Phys.*, 1983, **79**, 926–935.

45 C. E. Wilmer, K. C. Kim and R. Q. Snurr, An Extended Charge Equilibration Method, *J. Phys. Chem. Lett.*, 2012, **3**, 2506–2511.

46 L. Zhang and J. I. Siepmann, Direct Calculation of Henry's Law Constants from Gibbs Ensemble Monte Carlo Simulations: Nitrogen, Oxygen, Carbon Dioxide and Methane in Ethanol, *Theor. Chem. Acc.*, 2006, **115**, 391–397.

47 E. Garcia-Perez, J. Parra, C. Ania, D. Dubbeldam, T. Vlugt, J. Castillo, P. Merkling and S. Calero, Unraveling the Argon Adsorption Processes in MFI-Type Zeolite, *J. Phys. Chem.*, 2008, **112**, 9976–9979.

48 D. Frenkel and B. Smit, *Understanding Molecular Simulation: from Algorithms to Applications*, Elsevier, Academic Press, 2002; vol. 1, pp. 1–638.

49 D. Burris and W. Sawyer, Addressing Practical Challenges of Low Friction Coefficient Measurements, *Tribol. Lett.*, 2009, **35**, 17–23.

50 S. Shree, A. George, T. Lehnert, C. Neumann, M. Benelajla, C. Robert, X. Marie, K. Watanabe, T. Taniguchi and U. Kaiser, High Optical Quality of MoS$_2$ Monolayers Grown by Chemical Vapor Deposition, *2D Mater.*, 2019, **7**, 015011.

51 S. Srivastava and Y. N. Mohapatra, Defect Density of States in Natural and Synthetic MoS$_2$ Multilayer Flakes, *J. Phys. D: Appl. Phys.*, 2022, **55**, 345101.

52 Z. He, R. Zhao, X. Chen, H. Chen, Y. Zhu, H. Su, S. Huang, J. Xue, J. Dai and S. Cheng, Defect Engineering in Single-Layer MoS$_2$ Using Heavy Ion Irradiation, *ACS Appl. Mater. Interfaces*, 2018, **10**, 42524–42533.

53 A. F. Ismail, K. C. Khulbe and T. Matsuura, Gas Separation Membranes, *Switz. Springer*, 2015, **10**, 973–978.

54 G. Levita and M. C. Righi, Effects of Water Intercalation and Tribochemistry on MoS$_2$ Lubricity: An Ab Initio Molecular Dynamics Investigation, *ChemPhysChem*, 2017, **18**, 1475–1480.

55 G. Levita, E. Molinari, T. Polcar and M. C. Righi, First-Principles Comparative Study on the Interlayer Adhesion and Shear Strength of Transition-Metal Dichalcogenides and Graphene, *Phys. Rev. B*, 2015, **92**, 085434.

56 M. Matsunaga, K. Hoshimoto and Y. Uchiyama, Frictional Behaviour of Molybdenum Disulphide in High Vacuum, *Wear*, 1972, **22**, 185–192.

57 M. Matsunaga and K. Hoshimoto, Frictional Behaviour of Molybdenum Disulphide in High Vacuum—Part II, *Wear*, 1976, **38**, 371–384.